

Anisotropic two-orbital Hubbard model: single-site versus cluster dynamical mean-field theory

Hunpyo Lee,¹ Yu-Zhong Zhang,^{1,2} Harald O. Jeschke,¹ and Roser Valentí¹

¹*Institut für Theoretische Physik, Goethe-Universität Frankfurt,
Max-von-Laue-Straße 1, 60438 Frankfurt am Main, Germany*

²*Department of Physics, Tongji University, Shanghai, 200092 P. R. China*
(Dated: July 20, 2021)

The anisotropic two-orbital Hubbard model with different bandwidths and degrees of frustration in each orbital is investigated in the framework of both single-site dynamical mean-field theory (DMFT) as well as its cluster extension (DCA) for clusters up to four sites combined with a continuous-time quantum Monte Carlo algorithm. This model shows a rich phase diagram which includes the appearance of orbital selective phase transitions, non-Fermi liquid behavior as well as antiferromagnetic metallic states. We discuss the advantages and drawbacks of employing the single-site DMFT with respect to DCA and the consequences for the physical picture obtained out of these calculations. Finally, we argue that such a minimal model may be of relevance to understand the nature of the antiferromagnetic metallic state in the iron-pnictide superconductors as well as the origin of the small staggered magnetization observed in these systems.

PACS numbers: 71.10.Fd, 71.27.+a, 71.30.+h, 71.10.Hf

I. INTRODUCTION

The multiorbital Hubbard Hamiltonian has been proposed¹ to be a suitable model for the description of a large variety of correlated electron transition metal compounds including nickelates, vanadates, and more recently iron pnictide and chalcogenide superconductors². While new interesting phases like orbital-selective metal-insulator phase transitions, coexistence of paramagnetic with antiferromagnetic phases or coexistence of Fermi liquid with non-Fermi liquid behavior have been predicted for this model, there is still a strong debate regarding the true nature of the phase diagram. The reason for that lies in the complexity of the multiorbital model which includes orbital degrees of freedom, crystal field splitting effects as well as the Hund's rule exchange coupling and also in the nature of the approaches used in order to investigate the model. In this work, we shall present a comparative investigation of the properties of the anisotropic two-orbital Hubbard model within the single-site dynamical mean field approximation (DMFT)³⁻⁵ as well as the dynamical cluster approximation (DCA)²⁶ where spatial fluctuations are included.

We will focus on three major phenomena related to the multiorbital Hubbard model. (i) Orbital selective phase transitions (OSPT) which have been discussed, for instance, in $\text{Ca}_{2-x}\text{Sr}_x\text{RuO}_4$ ^{6,7} and recently in iron-based superconductors^{8,9} in the framework of DMFT and density functional theory (DFT) calculations. Within single-site DMFT it has been shown that the presence of OSPT is dependent on various effects like the existence of inequivalent bandwidths at integer filling¹⁰⁻¹³, the presence of crystal field splitting at non-integer filling¹⁵, the absence of interorbital hybridization¹⁴ as well as the appearance of different number of degenerate orbitals¹⁶. Nevertheless, it is unclear how these features are modified if spatial fluctuations are included in the calculations.

For instance, the single-site DMFT cannot capture the Slater physics caused by nesting effects as is the case in the spin-Peierls system TiOCl ^{17,18} where dimerization is important. (ii) Appearance of non-Fermi-liquid (FL) behavior. Non-FL behavior is present in the single-site DMFT calculations for the multiorbital^{20,21} Hubbard model and in the four-site cellular-DMFT (CDMFT) studies for the one-orbital Hubbard model^{22,23}. Based on the mentioned calculations, the mechanism of non-FL behavior is attributed to the ferromagnetic correlation between orbitals (Hund's coupling) in the case of multiorbital systems, while intersite antiferromagnetic correlations caused by the Coulomb repulsion are suggested as the driving mechanism in the one-orbital case. In an attempt to consider the effect of spatial fluctuations in the multiorbital Hubbard model, we investigated recently the mechanism of non-FL behavior^{24,25} within DCA. This study is developed further in the present work. (iii) Finally, we investigate the competing effect of frustrated orbitals in a multiorbital Hubbard model. Such a study has been motivated by the intensively discussed controversy about the origin of the observed reduced magnetic moment in Fe-based superconductors⁸ and the possible relation to the multiorbital nature of the system. Bandstructure calculations together with downfolding for various families of iron-based SC compounds show that weakly frustrated d_{xy} , d_{z^2} and highly frustrated $d_{yz/zx}$, $d_{x^2-y^2}$ orbitals coexist^{32,33}. We will show in what follows that competition of frustrated with non-frustrated orbitals induces an antiferromagnetic metallic phase with a reduced ordered magnetic moment^{8,25}, as observed in iron-based superconductors.

In section II we present the model and numerical methods considered which include the single-site DMFT, DCA and the continuous-time QMC algorithm as impurity solver. In section III, we discuss the appearance of orbital selective phase transitions and non-Fermi liquid behav-

ior for two models: **(I)** the half-filled two-orbital Hubbard model with unequal bandwidths on the square lattice in the framework of a four-site DCA paramagnetic (PM) solution and **(II)** the half-filled two-orbital Hubbard model on the Bethe lattice with one frustrated orbital and one unfrustrated orbital using the single-site DMFT with AF ordering. In this model we find an antiferromagnetic metallic phase as well as a reduced staggered magnetization as a consequence of competing frustration effects. Finally, in section IV we summarize our findings.

II. MODEL AND METHODS

We consider the anisotropic two-orbital Hubbard model with nearest- and next-nearest- hopping matrix elements:

$$H = - \sum_{\langle ij \rangle m \sigma} t_m c_{im\sigma}^\dagger c_{jm\sigma} - \sum_{\langle ij' \rangle m \sigma} t'_m c_{im\sigma}^\dagger c_{j'm\sigma} + U \sum_{im} n_{im\uparrow} n_{im\downarrow} + \sum_{i\sigma\sigma'} (U' - \delta_{\sigma\sigma'} J_z) n_{i1\sigma} n_{i2\sigma'} \quad (1)$$

where $c_{im\sigma}$ ($c_{im\sigma}^\dagger$) is the annihilation (creation) operator of an electron with spin σ at site i and orbital m . t_m (t'_m) is the hopping matrix element between site i and nearest-neighbor site j (next-nearest-neighbor site j'). U and U' are intraorbital and interorbital Coulomb repulsion integrals, respectively, and $J_z n_{i1\sigma} n_{i2\sigma}$ is the Ising-type Hund's rule coupling term. In our calculations we set $U' = \frac{U}{2}$ and $J_z = \frac{U}{4}$ in order to fulfill the condition $U = U' + 2J_z$ and evaluate the model with the single-site DMFT and four-site DCA methods combined with a continuous-time QMC algorithm.

Even though DCA can be considered as superior to the single-site DMFT method, both approaches are faced with certain advantages and drawbacks. While the single-site DMFT ignores spatial fluctuations, a notorious fermionic sign problem present in the QMC calculations disappears even in the frustrated systems with next nearest-neighbor hopping t' . On the other hand, while short-range spatial fluctuations are considered in the four-site DCA approach, the QMC calculations encounter a serious fermionic sign problem for the frustrated model²⁸. For these reasons, we first consider the anisotropic two-orbital model with different bandwidths t_m and no frustration $t'_m = 0$ on the square lattice at half-filling within the four-site DCA method (model **(I)** above). Although a mild fermionic sign problem with average sign around $\langle s \rangle = 0.98$ is observed, we believe that the results are numerically reliable.

In the DCA method the reduced Brillouin zone (BZ) is determined by dividing the total BZ with respect to the number of sites and the self-energies for the different cluster momenta are calculated – analogous to the DMFT equation – on the reduced BZ by considering the same assumption as in DMFT where the self-energy is constant in the (reduced) Brillouin zone. The DCA

self-consistent equations for each cluster momentum with $\mathbf{K} = (0, 0), (0, \pi), (\pi, 0)$ and (π, π) are given as

$$\bar{G}_\sigma(\mathbf{K}, i\omega_n) = \frac{1}{N} \sum_{\tilde{\mathbf{K}}} \frac{1}{i\omega_n + \mu - \epsilon_{\mathbf{K}+\tilde{\mathbf{K}}} - \Sigma_\sigma(\mathbf{K}, i\omega_n)} \quad (2)$$

where N is the number of sites, μ is the chemical potential, $\epsilon_{\mathbf{K}+\tilde{\mathbf{K}}}$ is the dispersion relation, ω_n is the Matsubara frequency, and the summation over $\tilde{\mathbf{K}}$ is calculated in each reduced Brillouin zone.

Next, we will study the anisotropic frustrated two-orbital Hubbard model on the Bethe lattice at half-filling with t_m and t'_m hopping matrix elements (model **(II)** above) by employing the single-site DMFT with an antiferromagnetic bath. The Néel state, in which the magnetization of A and B sublattices are in opposite directions, is included in the model and the DMFT self-consistency equations are given as

$$G_{0,A,\sigma}^{-1} = i\omega_n + \mu - t_m^2 G_{B,\sigma} - t_m'^2 G_{A,\sigma}, \quad (3)$$

$$G_{0,B,\sigma}^{-1} = i\omega_n + \mu - t_m^2 G_{A,\sigma} - t_m'^2 G_{B,\sigma}, \quad (4)$$

The sign problem is absent in the single-site impurity calculations, and the converged impurity Green's functions in both cases are determined after several iterations.

Two possible continuous-time (diagrammatic) QMC algorithms for solving the DMFT and DCA equations have been proposed. One is based on an expansion in the impurity-bath hybridization Δ ^{34,35} term – also called strong-coupling approach – and the other one is based on an expansion in the interaction term U ^{36–38}, denoted as weak-coupling approach. Unlike a determinant QMC method³⁹ which includes the artificial Trotter error caused by discretization of the imaginary time, this error is not present in the continuous-time QMC algorithms except as numerical noise. In addition, since the matrix sizes of both diagrammatic QMC methods are smaller than that of the determinant QMC method, it is possible to access the low temperature regime. For our study we employ the weak-coupling QMC method. The reason for this choice lies in the computational effort. While the strong-coupling QMC method for the single-site impurity problem of multiorbital systems has advantages like the possibility of considering the full Hund's rule coupling term without any fermionic sign problem and also the calculation at very low temperatures in strong-coupling regions, the numerical effort of such an approach increases rapidly with the number of cluster sites N as 2^{2N} . Therefore, in the multiorbital cluster systems the strong-coupling QMC method is computationally extremely expensive. On the other hand, the weak-coupling QMC method contains less numerical burden because the matrix size increases only linearly with N .

III. RESULTS

A. Orbital selective phase transitions and non-Fermi liquid behavior in the four-site DCA calculations

In this section, we present results which demonstrate the appearance of OSPT and non-FL behavior in the half-filled two-orbital Hubbard model with different hopping t_m in each orbital m on the square lattice (model **(I)**) by employing the four-site DCA calculations with paramagnetic bath. The hopping t_m of the narrow and wide bands are $t_1 = 0.5$ and $t_2 = 1.0$, respectively, and the temperature considered is $T/t_2 = 0.1$. In order to

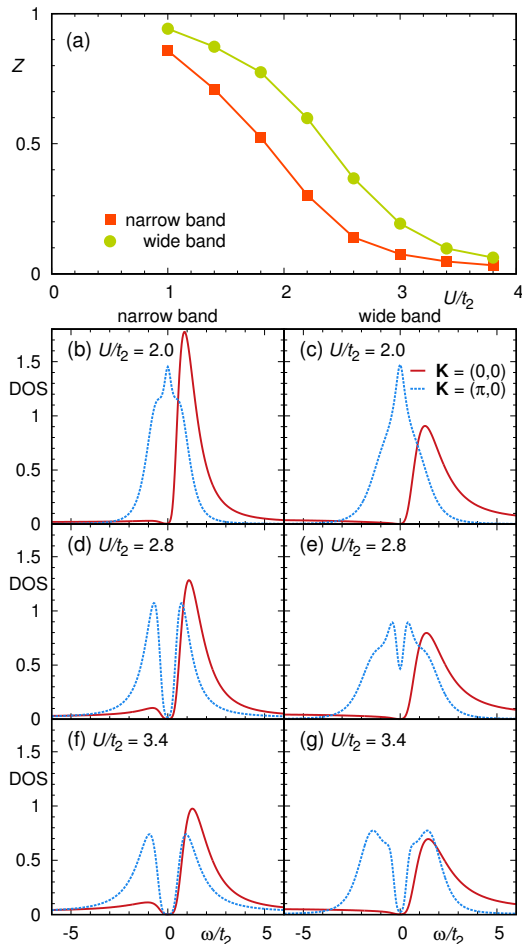


FIG. 1. (a) The quasiparticle weight $z_{\mathbf{K}}$ at $\mathbf{K} = (\pi, 0)$ as a function of U/t_2 for the narrow and wide bands. The spectral functions at $T/t_2 = 0.1$ for (b)-(c) $U/t_2 = 2.0$, (d)-(e) $U/t_2 = 2.8$, and (f)-(g) $U/t_2 = 3.4$ in the four-site dynamical cluster approximation (DCA) calculation.

investigate the existence of the OSPT, we first explore the quasiparticle weight $z_{\mathbf{K}}$ as a function of U/t_2 , which is given as $z_{\mathbf{K}} \approx [1 - \frac{\text{Im}\Sigma(\mathbf{K}, i\omega_0)}{\omega_0}]^{-1}$, where ω_0 is the lowest Matsubara frequency and \mathbf{K} is the momentum sector. The effective mass ratio, which is defined as $z_{\mathbf{K}}^{-1}$, gives in-

formation on correlation effects. As is well known, correlation is the driving force for a transfer of spectral weight from the coherent peak at the Fermi level ($\omega/t_2 = 0$) to incoherent peaks. This means that the quasiparticle weight $z_{\mathbf{K}}$ at the Fermi surface $\mathbf{K} = (\pi, 0)$ should be suppressed in a Mott insulating state due to enhancement of the effective mass. The results are shown in Fig. 1 (a). The quasiparticle weight $z_{\mathbf{K}}$ at $\mathbf{K} = (\pi, 0)$ in the narrow band is suppressed around $U/t_2 = 2.8$, while it remains large in the wide band. We can denote this feature as an orbital-selective phase where metallic and insulating states coexist between $U/t_2 = 2.8$ and 3.2 . In order to observe the OSPT more clearly at momentum sectors $\mathbf{K} = (0, 0)$ and $(\pi, 0)$, we plot in Figs. 1 (b)-(g) the spectral functions for $U/t_2 = 2.0, 2.8$ and 3.4 , where the maximum entropy method was used for analytical continuation. The spectral functions at $\mathbf{K} = (0, 0)$ show a band-insulator, while at $\mathbf{K} = (\pi, 0)$ they indicate metallic states in the weak-coupling region $U/t_2 = 2.0$ in both bands like in results obtained from non-interacting four-site DCA in the single-band Hubbard model⁴⁰. Upon increasing the interaction we find that the spectral functions indicating a band insulator at $\mathbf{K} = (0, 0)$ are almost unchanged. On the other hand, we observe that for $U/t_2 = 2.8$ the gap is completely opened at $\mathbf{K} = (\pi, 0)$ in the narrow band, while a finite density of states around the Fermi level remains in the wide band, clearly showing the coexistence of an insulator and a metal in this two-orbital system as displayed in Figs. 1 (d)-(e). In the strong-coupling region with $U/t_2 = 3.4$ in Figs. 1 (f)-(g), both phases at $\mathbf{K} = (\pi, 0)$ are insulating and the gap in the narrow band is larger than that in the wide band. This means that between $U/t_2 = 2.8$ and 3.4 a Mott metal-insulator transition at $\mathbf{K} = (\pi, 0)$ occurs in the wide band, while the narrow band is already in the insulating state; at the same time, a band insulator is sustained at $\mathbf{K} = (0, 0)$, regardless of the strength of the interaction U/t_2 .

Next, we plot the self-energies as a function of real frequency in Figs. 2 (a)-(h) to show the FL, non-FL and Mott insulating behavior clearly. The analytical continuation of the self-energy suggested by Wang et al.⁴¹ has been used. Here we briefly introduce the method: at high frequency ω_n the self-energy at half-filling should behave as $\Sigma(i\omega_n) \sim \frac{U^2}{4\omega_n}$. In order to perform the Fourier transformation of $\Sigma(i\omega_n)$, we need to take into account the correction of the high frequency tail as

$$\Sigma(\tau) \sim \frac{1}{\beta} \left(\sum_{n=-N_h}^{N_h} e^{-i\omega_n\tau} \Sigma(i\omega_n) + \sum_{n=-\infty}^{\infty} e^{-i\omega_n\tau} \frac{4}{U^2\omega_n} - \sum_{n=-N_h}^{N_h} e^{-i\omega_n\tau} \frac{4}{U^2\omega_n} \right) \quad (5)$$

where $\frac{1}{\beta} \sum_{n=-\infty}^{\infty} e^{-i\omega_n\tau} \frac{1}{i\omega_n} = -0.5$ and N_h is the highest number of Matsubara frequencies. Here, $\Sigma(\tau)$ is inserted into the maximum entropy equations to obtain

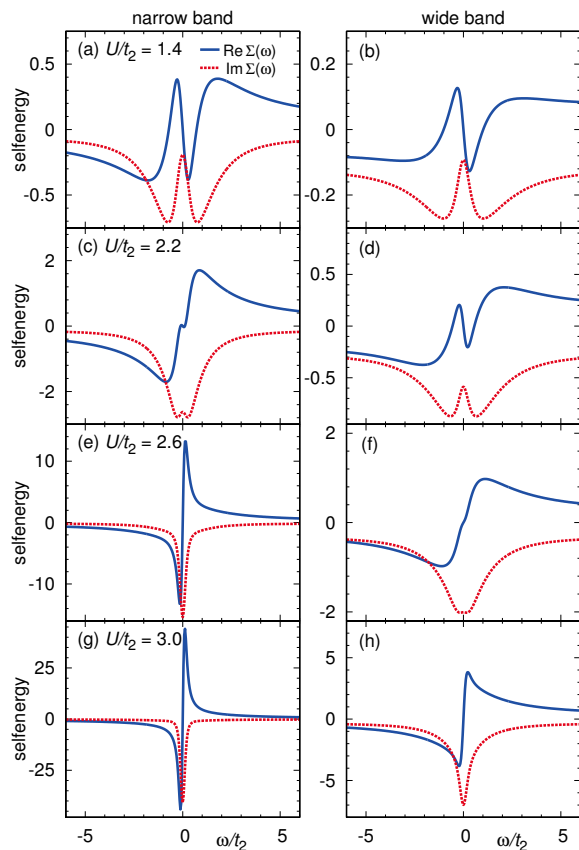


FIG. 2. Self-energies at the Fermi surface $\mathbf{K} = (\pi, 0)$ as a function of real frequency ω/t_2 at $T/t_2 = 0.1$ for the narrow and wide bands in the four-site DCA calculations: (a) and (b) $U/t_2 = 1.4$, (c) and (d) $U/t_2 = 2.2$, (e) and (f) $U/t_2 = 2.6$, and (g) and (h) $U/t_2 = 3.0$.

$\text{Im}\Sigma(\omega)$, where ω is the real frequency. $\text{Re}\Sigma(\omega)$ is then calculated by the Kramers-Kronig relation.

In the weak-coupling region, $U/t_2 = 1.4$, Figs. 2 (a)-(b) show that the imaginary part of the self-energy approaches zero as $\omega \rightarrow 0$ for both orbitals indicating FL states. As the interaction is increased, a non-FL state in the narrow band coexists with a FL state in the wide band as shown in Figs. 2 (c)-(d). By further increasing U/t_2 , the narrow band shows a Mott insulating behavior where $\text{Im}\Sigma(\omega)$ diverges at $\omega = 0$ (Fig. 2 (e)), while the wide band is still metallic with non-FL behavior (see Fig. 2 (f)). In the strong-coupling region $U/t_2 = 3.0$ in Figs. 2 (g)-(h), divergences of the imaginary part of the self-energy in both orbitals indicate a complete Mott insulating state.

B. OSPT and small magnetic moment in the single-site DMFT calculation

We proceed now to the analysis of the anisotropic two-orbital Hubbard model with frustrated and unfrustrated orbitals at half-filling using the two-sublattice single-site

DMFT with antiferromagnetic bath. In our calculations, the temperature is set to $T/t = 1/16$. The next nearest neighbour hopping is $t'/t = 0$ for the unfrustrated orbital and $t'/t = 0.65$ for the frustrated orbital with $t = 1.0$. We first evaluate the OSPT behavior of this model with the single-site DMFT, as we did within the four-site DCA approach in the former section. We observe that a band insulator is present since the source of the gap opening is not only the Coulomb interaction but also the magnetization of the AF solution. Therefore, the change of the effective mass – which is related to the quasiparticle weight z – is very small in contrast to the case of a Mott insulator. Therefore, we employ the DOS at Fermi level $\rho(\omega = 0)$ to identify the OSPT as is shown in Fig. 3. The results were obtained through analytical continuation applying the maximum entropy method and we performed around 10^7 QMC samplings and checked the results through a Pade approximation in order to ensure the reliability of the results. The gap opening is clearly observed around $U_{c_1}/t = 1.9$ in the unfrustrated orbital, while the metallic state is still present in the frustrated orbital. As the interaction is increased, a metal-insulator transition in the frustrated orbital appears around $U_{c_2}/t = 2.9$. Between $U_{c_1}/t < U/t < U_{c_2}/t$ we find a coexistence region of metallic and insulating states as a clear evidence of OSPT behavior. Comparing our results of Fig. 3 with those obtained with the single-site DMFT with a paramagnetic solution in the two-orbital Hubbard model with different bandwidths¹⁰, we find that in both cases the spectral densities $\rho(\omega = 0)$ decay suddenly to zero in the narrow (unfrustrated) band and the values in the wide (frustrated) bands are similar around U_{c_1} . The difference between these two results is that $\rho(\omega = 0)$ for the frustrated orbital of our system also drops to zero at U_{c_2} , while it decreases smoothly in the single-site DMFT calculation with paramagnetic solution¹⁰. We believe that this is due to the different mechanisms of the gap opening in each system.

The present model is also relevant for understanding the magnetic behavior of the iron-pnictide superconductors. Since the discovery of high- T_c superconductivity in iron pnictides in 2008², a lot of studies have been performed to find the mechanism of pairing in these materials^{42–44}. Unlike the high- T_c cuprate superconductors, whose parent compounds are antiferromagnetic insulators, an ordered antiferromagnetic metallic state with small magnetic moment is detected in iron pnictides. Density functional theory calculations on iron pnictides overestimate the values of the ordered magnetic moment compared with experimental results^{45–48}. Only by artificially considering a negative U or by employing a specific double counting correction within LDA+ U ^{49,50} can these values be reduced. Even though some DFT+DMFT calculations including quantum fluctuations have been performed, the mechanism of the small magnetic moment is still controversial^{51–63}. Here, within model (II) we discuss a possible mechanism for the small magnetic moment in iron pnictides and the presence of a metallic an-

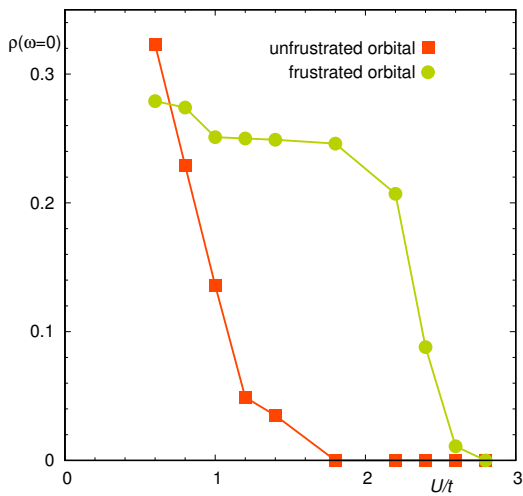


FIG. 3. The density of states $\rho(\omega = 0)$ at the Fermi level as a function of U/t for the unfrustrated and frustrated orbitals in the single-site dynamical mean field theory (DMFT) calculations.

tiferromagnetic state.

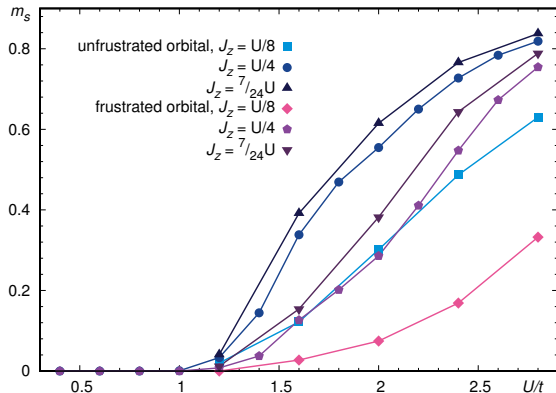


FIG. 4. Magnetization as a function of U/t with different values of J_z in the single-site DMFT calculations.

In our former studies, we proposed the coupling between frustrated and unfrustrated orbitals in a multi-orbital Hubbard model as the possible mechanism for the small magnetic moment observed in iron pnictides⁸. Based on the minimal two-orbital Hubbard model presented above, we found⁸ a continuous metal to insulator phase transition as well as a continuous magnetic phase transition for an Ising-Hund's rule coupling of $J_z = U/4$. The reduced ordered magnetic moment is shown in Fig. 4 as a function of U/t . We observe at a critical U/t a smooth increase of the magnetic moment, which is in contrast to the first order phase transition behavior observed in the one-orbital frustrated Hubbard model⁶⁴. In order to show that the results are independent of the choice of J_z we also show in Fig. 4 the magnetization for $J_z = 7U/24$, $U/8$ and $U/4$ with the constraint of $U = U' + 2J_z$. As the interaction is increased, the mag-

netization in all cases increases smoothly and in the intermediate interaction regime small magnetizations are observed.

IV. SUMMARY

In the present work we have explored the properties of two models. **(I)** The two-orbital Hubbard model with unequal bandwidths on the square lattice by employing the four-site DCA and **(II)** the two-orbital Hubbard model with a frustrated and an unfrustrated orbital on the Bethe lattice by using the single-site DMFT method. The DCA and DMFT equations were solved using a continuous-time QMC algorithm. The above choice of systems and methods explicitly avoids the fermionic sign problem in the QMC calculations. We find that both models show a rich phase diagram as a function of interaction strength which includes the appearance of orbital selective phase transitions, non-Fermi liquid behavior as well as antiferromagnetic metallic states.

Using the four-site DCA method with a PM solution for the two-orbital Hubbard model with different bandwidths (model **(I)**) we find that while the system behaves as a band insulator in the $K=(0,0)$ sector of the Brillouin zone, it undergoes an orbital selective phase transition in the $K=(\pi,0)$ sector. The system in the $K=(\pi,0)$ sector shows FL behavior for both orbitals in the weak-coupling region. As the interaction is increased, a non-FL state for the narrow band coexists with a FL behavior of the wide band. In the intermediate-coupling regime the non-FL behavior is changed into a Mott insulating state where the electrons are completely localized in the narrow band, while the metallic state with non-FL behavior is still observed in the wide band. In the strong-coupling region the spectral weight in each orbital shows a gap at the Fermi level, indicating a Mott insulating state in both orbitals. The observation of an OSPT in the intermediate region is due to the different electron localization in the orbitals. The non-FL behavior is also present due to weakly ordered states with AF correlations between sites and FM correlations between orbitals in the metallic regions.

Next, using the single-site DMFT with an AF solution, we studied model **(II)** and found that the critical interaction U for a metal-insulator phase transition are $U_{c_1}/t = 1.9$ and $U_{c_2}/t = 2.9$ for the unfrustrated and frustrated orbitals, respectively. This is a clear evidence of coexistence of two phases between the two critical U values. An OSPT is observed in this system since the strength of electron localization in both orbitals is different due to the unequal orbital frustration. The AF states are a key to the gap opening and the nature of the insulating state is that of a band insulator. Finally, such a minimal model may be of relevance to understand the nature of the antiferromagnetic metallic state in the iron-pnictide superconductors as well as the origin of the small staggered magnetization observed in these systems

since we measure the magnetization in each orbital and find that the magnetization only increases smoothly as a function of the interaction strength in the antiferromagnetic metallic state.

V. ACKNOWLEDGEMENTS

We would like to thank H. Monien and C. Gros for useful discussions and we gratefully acknowledge financial support from the Deutsche Forschungsgemeinschaft through grants FOR 1346 and SPP 1458 and from the Helmholtz Association through grant HA216/EMMI.

-
- ¹ M. Imada, A. Fujimori, and Y. Tokura, *Rev. Mod. Phys.* **70**, 1039 (1998).
- ² Y. Kamihara, T. Watanabe, M. Hirano, and H. Hosono, *J. Am. Chem. Soc.* **130**, 3296 (2008).
- ³ W. Metzner and D. Vollhardt, *Phys. Rev. Lett.* **62**, 324 (1989).
- ⁴ A. Georges, G. Kotliar, W. Krauth, and M. J. Rozenberg, *Rev. Mod. Phys.* **68**, 13 (1996).
- ⁵ G. Kotliar and D. Vollhardt, *Phys. Today* **57**, 53 (2004).
- ⁶ V.I. Anisimov, I. A. Nekrasov, D.E. Kondakov, T.M. Rice, and M. Sigrist, *Eur. Phys. J. B* **25**, 191 (2002).
- ⁷ Z. Fang, N. Nagaosa, and K. Terakura, *Phys. Rev. B* **69**, 045116 (2004).
- ⁸ H. Lee, Y. Z. Zhang, H. O. Jeschke, and R. Valentí, *Phys. Rev. B* **81**, 220506(R) (2010).
- ⁹ H. Oh, D. Shin, and H. J. Choi, arXiv:1012.2224 (unpublished).
- ¹⁰ C. Knecht, N. Blümer, and P. G. J. Van Dongen, *Phys. Rev. B* **72**, 081103(R) (2005).
- ¹¹ A. Liebsch, *Phys. Rev. B* **70**, 165103 (2004).
- ¹² R. Arita and K. Held, *Phys. Rev. B* **72**, 201102(R) (2005).
- ¹³ A. Koga, N. Kawakami, T. M. Rice, and M. Sigrist, *Phys. Rev. Lett.* **92**, 216402 (2004).
- ¹⁴ L. de'Medici, A. Georges, and S. Biermann, *Phys. Rev. B* **72**, 205124 (2005).
- ¹⁵ P. Werner and A. J. Millis, *Phys. Rev. Lett.* **99**, 126405 (2007).
- ¹⁶ L. de'Medici, S. R. Hassan, M. Capone, and X. Dai, *Phys. Rev. Lett.* **102**, 126401 (2009).
- ¹⁷ T. Saha-Dasgupta, A. Lichtenstein, and R. Valentí, *Phys. Rev. B* **71**, 153108 (2005).
- ¹⁸ T. Saha-Dasgupta, S. Glawion, M. Sing, R. Claessen, and R. Valentí, *New J. Phys.* **9**, 380 (2007).
- ¹⁹ J. Schafer, M. Hoinkis, E. Rotenberg, P. Blaha, and R. Claessen, *Phys. Rev. B* **72**, 155115 (2005).
- ²⁰ A. Liebsch, *Phys. Rev. Lett.* **95**, 116402 (2005).
- ²¹ S. Biermann, L. de'Medici, and A. Georges, *Phys. Rev. Lett.* **95**, 206401 (2005).
- ²² Y.-Z. Zhang and M. Imada, *Phys. Rev. B* **76**, 045108 (2007).
- ²³ H. Park, K. Haule, and G. Kotliar, *Phys. Rev. Lett.* **101**, 186403 (2008).
- ²⁴ H. Lee, Y.-Z. Zhang, H. O. Jeschke, R. Valentí, and H. Monien, *Phys. Rev. Lett.* **104**, 026402 (2010).
- ²⁵ H. Lee, Y.-Z. Zhang, H. O. Jeschke, and R. Valentí, arXiv:1011.0334 (unpublished).
- ²⁶ T. Maier, M. Jarrell, T. Pruschke, and M. Hettler, *Rev. Mod. Phys.* **77**, 1027 (2005).
- ²⁷ K. Bouadim, G. G. Batrouni, and R. T. Scalettar, *Phys. Rev. Lett.* **102**, 226402 (2009).
- ²⁸ E. Gull, P. Werner, O. Parcollet, and M. Troyer, *Europhys. Lett.* **82**, 57003 (2008).
- ²⁹ E. Gull, P. Werner, X. Wang, M. Troyer, and A. J. Millis, *Europhys. Lett.* **84**, 37009 (2008).
- ³⁰ A. Fuhrmann, S. Okamoto, H. Monien, and A. J. Millis, *Phys. Rev. B* **75**, 205118 (2007).
- ³¹ Clarina de la Cruz, *et al.*, *Nature* **453**, 899 (2008).
- ³² T. Miyake *et al.*, *J. Phys. Soc. Jpn.* **79**, 044705 (2010).
- ³³ K. Foyevtsova, J. Ferber, M. Aichhorn *private communication*.
- ³⁴ P. Werner, A. Comanac, L. de'Medici, M. Troyer, and A. J. Millis, *Phys. Rev. Lett.* **97**, 076405 (2006).
- ³⁵ P. Werner and A. J. Millis, *Phys. Rev. B* **74**, 155107 (2006).
- ³⁶ A. N. Rubtsov, V. V. Savkin, and A. I. Lichtenstein, *Phys. Rev. B* **72**, 035122 (2005).
- ³⁷ H. Lee, G. Li, and H. Monien, *Phys. Rev. B* **78**, 205117 (2008).
- ³⁸ F. F. Assaad and T. C. Lang, *Phys. Rev. B* **76**, 035116 (2007).
- ³⁹ J. E. Hirsch and R. M. Fye, *Phys. Rev. Lett.* **56**, 2521 (1986).
- ⁴⁰ K. Haule and G. Kotliar, *Phys. Rev. B* **76**, 104509 (2007).
- ⁴¹ X. Wang, E. Gull, L. de'Medici, M. Capone, and A. J. Millis, *Phys. Rev. B* **80**, 045101 (2009).
- ⁴² I. I. Mazin, D. J. Singh, M. D. Johannes, and M. H. Du, *Phys. Rev. Lett.* **101**, 057003 (2008).
- ⁴³ K. Kuroki, S. Onari, R. Arita, H. Usui, Y. Tanaka, H. Kontani, and H. Aoki, *Phys. Rev. Lett.* **101**, 087004 (2008).
- ⁴⁴ P. J. Hirschfeld, *Physics* **2**, 100 (2009).
- ⁴⁵ I. I. Mazin, M.D. Johannes, L. Boeri, K. Koepernik, and D. J. Singh, *Phys. Rev. B* **78**, 085104 (2008).
- ⁴⁶ I. Opahle, H. C. Kandpal, Y. Zhang, C. Gros, and R. Valentí, *Phys. Rev. B* **79**, 024509 (2009).
- ⁴⁷ Y.-Z. Zhang, H. C. Kandpal, I. Opahle, H. O. Jeschke, and R. Valentí, *Phys. Rev. B* **80**, 094530 (2009).
- ⁴⁸ Y.-Z. Zhang, I. Opahle, H.O. Jeschke, and R. Valentí, *Phys. Rev. B* **81**, 094505 (2010).
- ⁴⁹ J. Ferber, Y.-Z. Zhang, H. O. Jeschke, and R. Valentí, *Phys. Rev. B* **82**, 165102 (2010).
- ⁵⁰ F. Cricchio, O. Grånäs, and L. Nordström, *Phys. Rev. B* **81**, 140403 (2010).
- ⁵¹ T. Yildirim, *Phys. Rev. Lett.* **101**, 057010 (2008).
- ⁵² Q. Si and E. Abrahams, *Phys. Rev. Lett.* **101**, 076401 (2008).
- ⁵³ M. J. Han, Q. Yin, W. E. Pickett, and S. Y. Savrasov, *Phys. Rev. Lett.* **102**, 107003 (2009).
- ⁵⁴ B. Schmidt, M. Siahatgar, and P. Thalmeier, *Phys. Rev. B* **81**, 165101 (2010).
- ⁵⁵ K. Haule, J. H. Shim, and G. Kotliar, *Phys. Rev. Lett.* **100**, 226402 (2008).
- ⁵⁶ L. Craco, M. S. Ladd, S. Leoni, and H. Rosner, *Phys. Rev. B* **78**, 134511 (2008).
- ⁵⁷ K. Haule and G. Kotliar, *New J. Phys.* **11**, 025021 (2009).

- ⁵⁸ S. L. Shornyakov, A. V. Efremov, N. A. Skorikov, M. A. Korotin, Y. A. Izyumov, V. I. Anisimov, A. V. Kozhevnikov, and D. Vollhardt, *Phys. Rev. B* **80**, 092501 (2009)
- ⁵⁹ H. Ishida and A. Liebsch, *Phys. Rev. B* **81**, 054513 (2010).
- ⁶⁰ E. Bascones, M. Calderon, and Valenzuela, *Phys. Rev. Lett.* **104**, 227201 (2010).
- ⁶¹ F. Yang, S. P. Kou, and Z. Y. Weng, *Phys. Rev. B* **81**, 245130 (2010).
- ⁶² T. Misawa, K. Nakamura, and M. Imada, *J. Phys. Soc. Jpn.* **80**, 023704 (2011).
- ⁶³ Z. P. Yin, K. Haule, and G. Kotliar, arXiv:1007.2867 (unpublished).
- ⁶⁴ R. Zitzler, N. H. Tong, T. Pruschke, and R. Bulla, *Phys. Rev. Lett.* **93**, 016406 (2004).